Materials Science & Engineering A 598 (2014) 387–395

Contents lists available at ScienceDirect

Materials Science & Engineering A

journal homepage: www.elsevier.com/locate/msea

# Cryogenic properties of Al–Mg–Sc–Zr friction-stir welds

D. Zhemchuzhnikova [a,*], S. Malopheyev [a], S. Mironov [b], R. Kaibyshev [a]

[a] Laboratory of the Mechanical Properties of Nanoscale Materials and Superalloys, Belgorod State University, Pobeda 85, Belgorod 308015, Russia
[b] Department of Materials Processing, Graduate School of Engineering, Tohoku University, 6-6-02 Aramaki-aza-Aoba, Sendai 980-8579, Japan

ARTICLE INFO

*Article history:*
Received 7 October 2013
Received in revised form
20 January 2014
Accepted 21 January 2014
Available online 30 January 2014

*Keywords:*
Aluminum alloys
Welding
Grain refinement
Mechanical characterization
Fracture

ABSTRACT

In this work, the effect of friction-stir welding (FSW) on the microstructure and cryogenic properties of an Al–Mg–Sc–Zr alloy was studied. The produced friction-stir joints demonstrated both excellent static and dynamic mechanical properties at cryogenic temperatures. The joint efficiency for the yield strength during transverse tensile tests was in the range of 95–100%, whereas the impacts fracture toughness in the stir zone was found to be superior compared with that in the base material. The high level of the mechanical properties was attributed to the preservation of $Al_3(Sc,Zr)$ dispersoids, extensive grain refinement and the breaking of the continuous grain boundary network of the coarse $Al_6Mn$ particles during FSW.



## 1. Introduction

Al–Mg alloys containing trace Sc and Zr are novel lightweight structural materials for high performance applications. Minor additions of Sc and Zr give rise to precipitation of coherent nano-scale $Al_3(Sc,Zr)$ dispersoids, which impart a significant strengthening effect and are very effective in the stabilizing of the grain structure, e.g., [1]. This combination of properties makes these materials very attractive for use at ambient and elevated temperatures. In addition, the superior strength and ductility of these materials have been demonstrated recently to also be very promising for cryogenic applications [2]. The successful utilization of these advanced alloys relies heavily on the availability of a welding process that produces sound joints. Conventional fusion welding of Al–Mg–Sc alloys has been shown to lead to considerable degradation of the material strength due to dissolution of the unique precipitates [3,4]. In this regard, friction-stir welding (FSW) is an innovative "solid-state" joining technology that appears to be particularly attractive for the joining of Al–Mg–Sc alloys. Due to the relatively low heat input associated with FSW, this technique enables the preservation of the fine coherent particles and thus ensures good functional properties of the joints involving Al–Mg–Sc alloys.

The superior properties of friction-stirred Al–Mg–Sc alloys at elevated and ambient temperatures are already well documented [3–15]. However, almost no attention has been paid to the performance of friction-stirred Al–Mg–Sc alloys in the cryogenic temperature range. To fill this gap in the scientific literature, this work examined the static as well as the dynamic mechanical properties of Al–Mg–Sc friction-stir joints at cryogenic temperatures and evaluated their respective microstructure-properties relationships.

## 2. Experimental

The program material used in the present investigation was a commercial Al–6.0Mg–0.35Mn–0.2Sc–0.1Zr (in wt%) alloy 1575C (in the Russian classification). The manufacturing details of this material have been described elsewhere [2]. Briefly, the material was produced by semi-continuous casting followed by homogenization annealing at 360 °C for 12 h. The samples obtained from this processing route are denoted as cast material. The cast material was then rolled at 360 °C to a total thickness reduction of 75%; the obtained samples are referred to as hot rolled material. To develop a broader view on the effect of FSW on the structure and properties of 1575C alloy, it was studied in both cast as well as hot rolled conditions.

The sheets of 10 mm in thickness studied were machined from both preprocessed materials and friction-stir butt welded using an AccuStir 1004 FSW machine. Depending on the material condition, the sheets were joined either along the main ingot axis or the rolling direction. The welding tool was fabricated from a tool steel and consisted of a shoulder having a diameter of 16 mm and a threaded pin tapered linearly from 6 mm at the tool shoulder to 4.8 mm at the pin tip; the pin depth was 6.5 mm. To ensure a full-thickness joining, double-side FSW was conducted. The welding process was performed at a tool rotational speed of 500 rpm, tool travel speed of 150 mm/min and a tool tilt angle of 2.5°. To maintain consistency with the FSW literature, the principal directions of the welding geometry are denoted as the welding direction (WD), transversal direction (TD) and normal direction (ND).

* Corresponding author. Tel./fax: +7 4 72 258 5456.
*E-mail address:* zhemchuzhnikova@bsu.edu.ru (D. Zhemchuzhnikova).

0921-5093/$ - see front matter © 2014 Elsevier B.V. All rights reserved.
http://dx.doi.org/10.1016/j.msea.2014.01.060

Microstructural observations were performed by optical microscopy, scanning electron microscopy (SEM), the electron-backscatter diffraction (EBSD) technique and transmission electron microscopy (TEM). The microstructural specimens were prepared by using standard metallographic techniques. The details of microstructural examinations are described elsewhere [2].

To evaluate the cryogenic properties of the produced joints as well as the stir zone material, tensile tests and U-notched Charpy impact tests were conducted in a temperature range from 20 °C to −196 °C. Two tensile specimens and one impact specimen were used for each material/temperature condition.

To examine the weld properties, transverse tensile tests were used. In this case, the tensile specimens were centered at the weld line; had a gauge section of 35 mm in length, 7 mm in width and 3 mm in thickness; and included all of the characteristic microstructural zones developed during the FSW process. To study the mechanical properties of the stir zone material only, longitudinal tensile tests were performed. These specimens were cut parallel to the weld centerline; had a gauge section of 16 mm in length, 3 mm in width and 1.5 mm in thickness; and included stir zone material only. In all cases, tension tests to failure were conducted at a constant cross-head velocity corresponding to a nominal strain rate of $2\times10^{-3}\,s^{-1}$ using an Instron 5882 testing apparatus equipped with an Instron 3119-408 cryogenic chamber.

The Charpy impact specimens were 55 mm long, 10 mm wide and 10 mm thick, and they had a 2-mm deep "U" notch placed either at the stir zone centerline or in the base material region. The impact tests were conducted in accordance with the standard ASTM E23 by using an Instron IMP460 machine with a capacity of 300 J.

## 3. Results

### 3.1. Microstructure

#### 3.1.1. Base material

The initial microstructure of the cast and hot-rolled materials has been described in detail in a previous work [2]. Briefly, the microstructure of the cast material consisted of equiaxed grains with a mean size of 22 μm (Fig. 1a). The grains contained almost no sub-boundaries, and the density of free dislocations was measured to be as low as $3\times10^{12}\,m^{-2}$. A characteristic feature of this material was a continuous network of relatively coarse $Al_6Mn$ particles arranged along the original grain boundaries (Fig. 1b). The nano-scale $Al_3(Sc,Zr)$ dispersoids were uniformly distributed in the grain interior (not shown).

The hot rolling resulted in significant compression of the original grains and the formation of the developed substructure (Fig. 1c). The deformation-induced boundaries typically exhibit a misorientation of less than 2° and were very closely spaced, with a mean intercept of ~0.3 μm. The density of free dislocations increased up to $4\times10^{13}\,m^{-2}$. Importantly, the original grain boundaries were found to be detached from the continuous grain-boundary network of $Al_6Mn$ particles [2]. However, the $Al_3(Sc,Zr)$ dispersoids exhibited no apparent changes, either in the morphology or in the size and volume fraction (Fig. 1d).

#### 3.1.2. Friction-stir welded material

The low magnification overviews of the transversal cross-sections of the friction-stir welds obtained in the cast and hot rolled materials are summarized in Fig. 2. The advancing and retreating sides of the welds are abbreviated as AS and RS, respectively. In this study, the double-sided FSW was applied in mutually opposite directions, and thus the AS and RS reversed from the upper to bottom surfaces of the welds. It is clear from the figure that the welds contained no evident volumetric defects. A distinct stir zone developed in each weld. The optical contrast was observed to be inhomogeneous within both stir zones, being relatively dark on the advancing side and the near-surface regions.

The microstructures that evolved in the stir zones of the cast as well as the hot-rolled materials were found to be broadly similar to each other. A typical example is illustrated in Fig. 3; the key microstructural parameters are summarized in Table 1. In both cases, the microstructures were dominated by completely recrystallized grains with a mean grain size of ~1 μm (Fig. 3, Table 1).

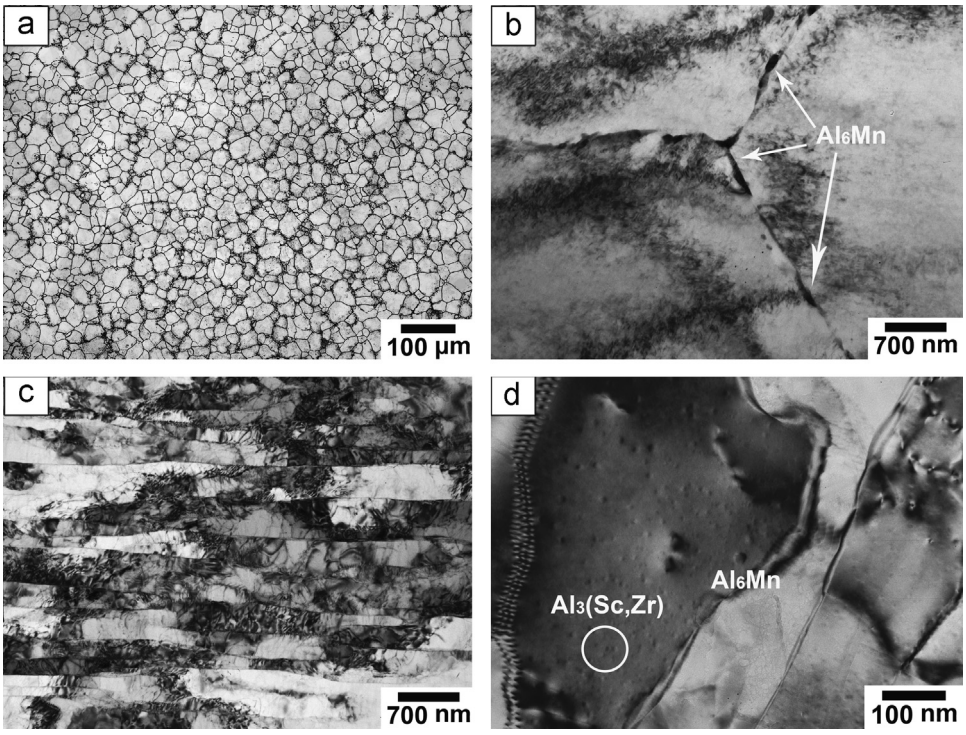


**Fig. 1.** Initial microstructure of the cast material (a, b) and the hot-rolled material (c, d). See Section 3.1.1 for details.

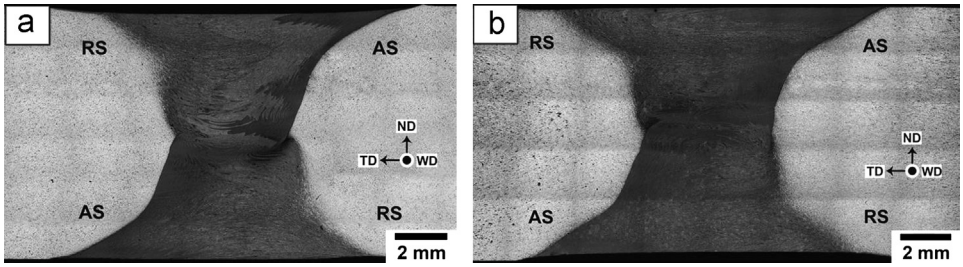


**Fig. 2.** Low-magnification overview of the transversal cross-sections of friction-stir welds obtained in the cast material (a) and hot-rolled material (b). The retreating and advancing sides of the welds are abbreviated as RS and AS, respectively.

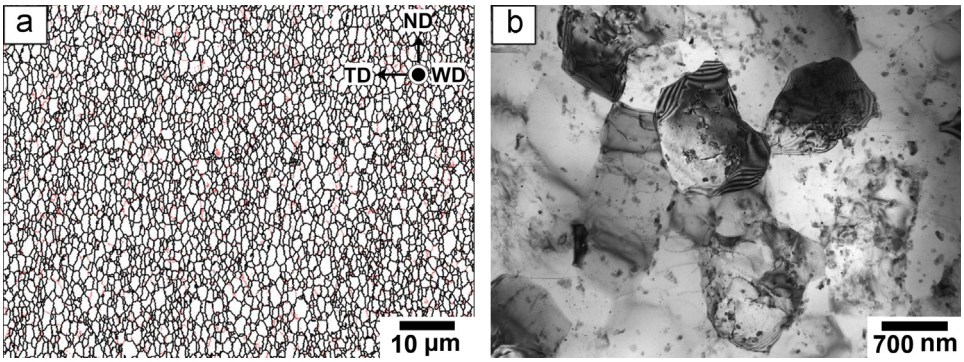


**Fig. 3.** Typical stir zone microstructure: grain-boundary EBSD map (a) and TEM image (b). In (a), low-angle boundaries ($2^\circ < \theta < 15^\circ$) and high-angle boundaries ($\theta > 15^\circ$) are depicted as red and black lines, respectively. Note: in this figure, the stir zone microstructure of the hot-rolled material is shown. See Section 3.1.2 for details. (For interpretation of the references to color in this figure legend, the reader is referred to the web version of this article.)

**Table 1**
Microstructure parameters of stir zone materials in cast and hot-rolled conditions.

| Material state | Microstructure parameters in stir zone | | |
|---|---|---|---|
| | Mean grain size, μm | HAB fraction, % | Dislocation density, $m^{-2}$ |
| Cast | 0.9 | 94 | $2 \times 10^{13}$ |
| Hot rolled | 1.1 | 93 | $2.6 \times 10^{13}$ |

The fraction of high-angle boundaries was as high as ~95% whereas the density of free dislocations was as low as $\sim 2.5 \times 10^{13}\ m^{-2}$ (Table 1). However, second phase particles did not exhibit any considerable changes, either in the morphology or in the volume fraction (Fig. 3b). Generally, the stir zone microstructures observed in this work agreed well with those reported in the scientific literature [3–15].

### 3.2. Microstructure–strength relationship

To evaluate the microstructure–strength relationship at ambient temperature, microhardness maps were measured in the weld zones of cast and hot-rolled materials, as shown in Fig. 4. For clarity, pin contours were also indicated in the figures by dotted lines.

In both cases, the microhardness distribution was inhomogeneous within the stir zone. An increased microhardness was observed in an overlapping area of the upper and lower FSW passes, as well as at the advancing side and in the near-surface areas of the stir zone. The microstructure in these locations is thought to be specific and requires additional study.

With the exception of these three areas, the microhardness in the stir zone of the cast material did not exhibit measurable changes compared with that in the initial condition (Fig. 4a). Considering the extensive grain refinement that occurred during the FSW process (compare Figs. 1a and 3), this result perhaps indicates that the grain-strengthening effect was small, if any effect was present.

The hot-rolled material in the preprocessed condition exhibited a relatively high microhardness level (Fig. 4b). The strengthening effect is thought to be primarily related with the formation of developed substructure and the high dislocation density (Fig. 1c). In the weld zone, however, a notable softening was observed (Fig. 4b). Remarkably, the softened area significantly exceeded the stir zone, also encompassing a heat affected zone (Fig. 4b). Considering preservation of nano-scale $Al_3(Sc,Zr)$ dispersoids (Fig. 3b), the softening effect was most likely attributable to the recovery and recrystallization in the weld zone, which eliminated the initial work-hardened microstructure [3–6]. Thus, the drastic grain refinement during FSW could not overbalance the substructure strengthening effect in the initial hot-rolled state.

Importantly, the stir zone microhardness was broadly similar in both studied conditions – cast as well as hot-rolled ones (compare Fig. 4a and b). This agrees well with the above microstructural observations and suggests that the initial material state has only a minor influence on the final stir zone microstructure.

### 3.3. Cryogenic properties

#### 3.3.1. Tensile properties of the joints

The effect of cryogenic temperature on the tensile behavior of friction-stir joints is shown in Fig. 5. Deformation diagrams for the respective base materials are also added to Fig. 5a and b for comparative purposes. The appearance of the welded specimens tensioned to failure at ambient temperature and at −196 °C is illustrated in Fig. 6; for simplicity, the black lines in the specimens delineate the stir zone.

In all cases, a decrease of the test temperature into the cryogenic range smoothed the deformation diagrams; in the base materials, this also significantly improved the ductility (Fig. 5a and b). As discussed in a previous work [2], these effects are thought to be associated with the suppression of the dynamic strain aging occurring at room temperature.

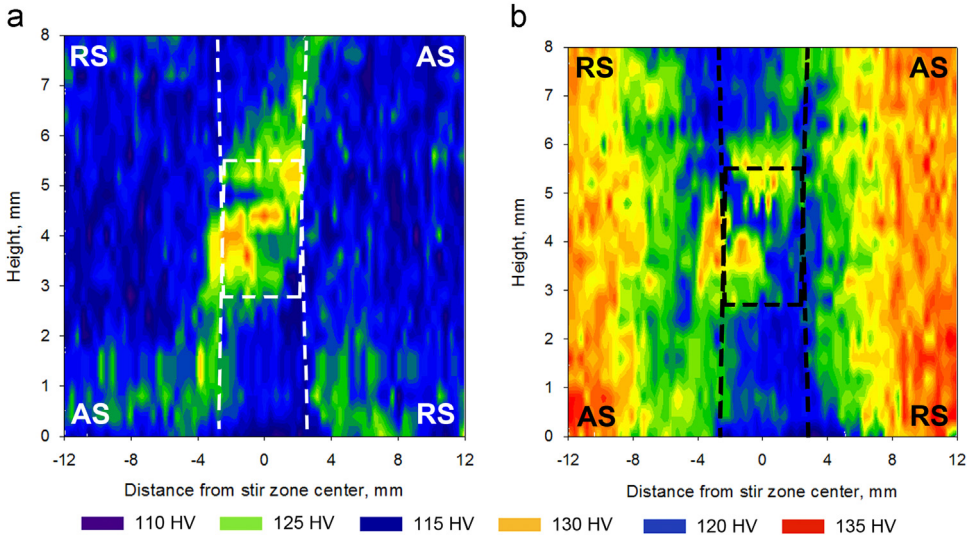


**Fig. 4.** Microhardness maps measured in the weld zone of cast (a) and hot-rolled (b) materials. Dotted lines indicate pin (for the upper and lower FSW passes). See Section 3.2 for details.

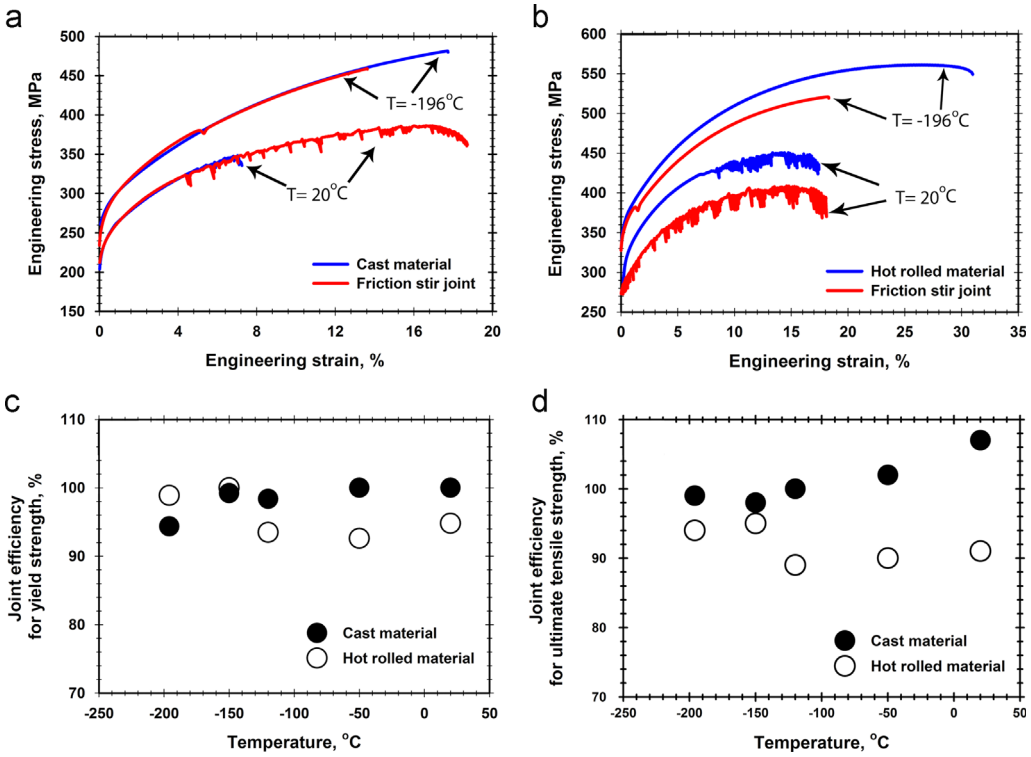


**Fig. 5.** The effect of temperature on the tensile properties: selected deformation diagrams for transverse tensile tests of preprocessed and friction-stir welded materials in cast (a) and hot rolled (b) conditions, and the joint efficiency for yield strength (c) and for ultimate strength (d). See Section 3.3.1 for details.

In the cast material, the joint efficiency of the friction-stir welds was close to 100% (Fig. 5c and d), with the failure typically occurring in the base material region (Fig. 6) over the entire studied temperature range. This observation was presumably related to local hardening in the stir zone (Fig. 4a) and the respective concentration of the tensile strain in the base material region.

In the hot-rolled state, the joint efficiency at ambient temperature was somewhat lower (~95%) (Fig. 5c and d) and the tensile specimens were fractured in the stir zone (Fig. 6a). This observation correlates well with the observed material softening in the stir zone (Fig. 4), as discussed in Section 3.2. With a decrease of the test temperature below −125 °C, however, the joint efficiency increased (Fig. 5c and d), and the joints also failed in the base material region (Fig. 6b). These observations indicate that the stir zone in this low temperature range had higher strength than the base material.

### 3.3.2. *Tensile behavior of the stir zone material*

To clarify the tensile behavior of the stir zone material, longitudinal tensile specimens were machined from the stir zone and tested at ambient and cryogenic temperatures, as presented in

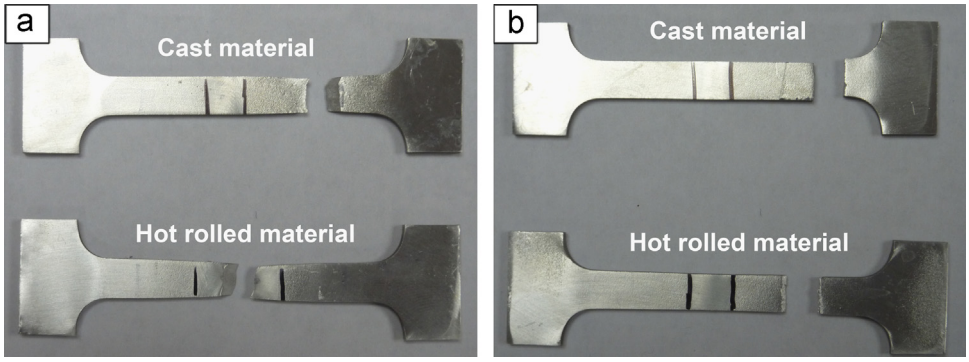


**Fig. 6.** Appearance of the welded specimens tensioned to failure at room temperature (a) and at −196 °C (b). The black lines indicate the weld borderlines.

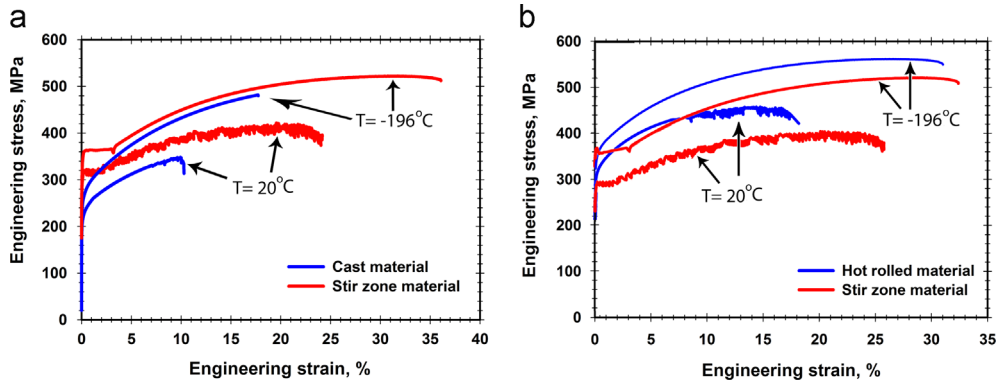


**Fig. 7.** Deformation diagrams for longitudinal tensile tests of the base material and the stir zone material in cast (a) and hot rolled (b) conditions. See Section 3.3.2 for details.

**Table 2**
Longitudinal tensile properties of the base material and the stir zone material at ambient and cryogenic temperatures.

| Material condition | | Tensile properties at 20 °C/−196 °C | | |
|---|---|---|---|---|
| | | Yield strength, MPa | Ultimate tensile strength, MPa | Ductility, % |
| Cast | Base material | 225/260 | 360/470 | 11/17 |
| | Stir zone | 315/355 | 410/520 | 24/36 |
| Hot rolled | Base material | 295/335 | 450/555 | 20/31 |
| | Stir zone | 290/365 | 390/520 | 26/33 |

Fig. 7 and Table 2. The tensile properties of the base materials were also shown for comparative purposes.

Note that the tensile behavior of the stir zone material in the cast and hot-rolled conditions was broadly similar to each other. The observed discrepancies appear to be within the experimental data scattering. It is apparent that there is broad similarity of the stir zone microstructures in both studied material conditions.

In the line with transverse tensile tests, the yield strength and ultimate tensile strength of the stir zone material exceeded those of the cast material in entire studied temperature range (Fig. 7a, Table 2). In the hot rolled condition, however, the preprocessed material generally demonstrated higher strength than the stir zone material (Fig. 7b). At very low temperatures, however, the deformation diagrams for the stir zone material were featured by a yield point (Fig. 7b). This effect promoted an increase of the yield stress and ultimately improved the respective joint efficiency up to almost 100% (Fig. 5c).

In this context, it is useful to consider the onset of plastic strain of the stir zone material in more detail. It is clear from Fig. 7 that this strain range was featured by a pronounced Luders strain. This phenomenon is relatively well documented in Al–Mg-based alloys [16,17]. It is well accepted to originate from strain localization within Luders bands and their subsequent propagation throughout the entire specimen gauge. In turn, the formation of the Luders bands is commonly believed to be related to an abrupt increase of the density of mobile dislocations.

To examine this idea, the structure evolved in the stir zone material after ~5% of tensile strain (which approximately corresponded to the end of the Luders site in Fig. 7) was studied in more detail. TEM observations (Fig. 8) showed that the dislocation density was indeed almost trebled achieving $\sim 8 \times 10^{13}$ m$^{-2}$. On the other hand, no evidence for deformation banding was found.

The abrupt increase of dislocation density is conventionally believed to be related either with unlocking of dislocations from the solute atmosphere or with rapid dislocation multiplications. Considering the fine-grained and almost dislocation-free nature of the stir zone material (Fig. 3b), however, the Luders strain in our case is thought to rather originate from rapid dislocation multiplication at the strain onset.

The dislocation multiplication is believed to be substantially influenced by cross slip. At cryogenic temperatures, however, the cross slip is expected to be suppressed, and thus the respective mechanism of dislocation multiplication should be inhibited. This should increase yield strength and finally produce dislocation

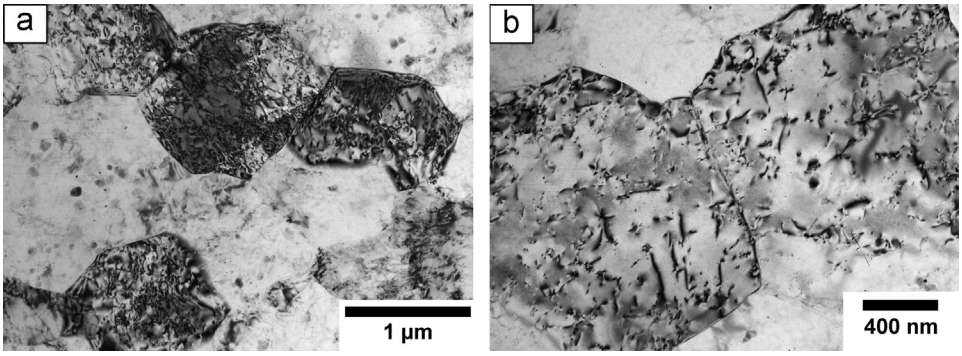


**Fig. 8.** Microstructure of the longitudinal stir zone specimens after tensile testing at −196 °C to engineering strain ~5%: low magnification (a) and high magnification (b) views.

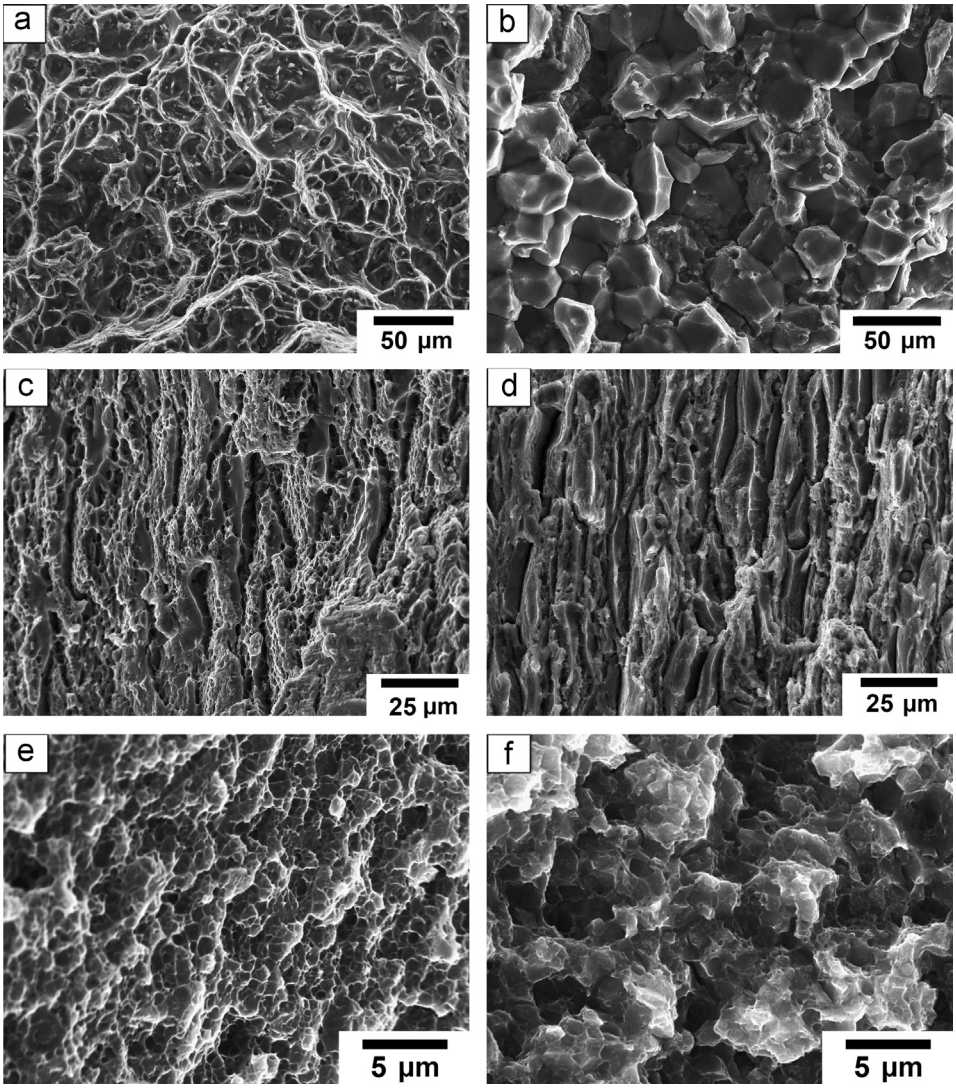


**Fig. 9.** SEM micrographs illustrating the effect of temperature on the fracture surface of longitudinal tensile specimens: cast material tested at 20 °C (a) and −196 °C (b), hot-rolled material tested at 20 °C (c) and −196 °C (d) and friction-stir welded cast material tested at 20 °C (e) and −196 °C (f). See Section 3.3.2 for details.

"avalanche". In turn, this additional strengthening may be responsible for increase of the joint efficiency for the yield strength of the hot rolled material up to almost 100% with decreasing temperature (Fig. 5c).

It is worth noting that the Luders strain was not observed during transverse tensile tests (Fig. 5a, b) despite some of the specimens being fractured in the stir zone (bottom part of Fig. 6a). This observation is thought to be related with relatively small volume fraction of the stir zone in the transverse tensile specimens (as noted in Section 2) and thus insufficient contribution of the Luders banding into global tensile behavior.

The typical SEM micrographs of the fractured surfaces of the longitudinal tensile specimens are shown in Fig. 9. Fractography of the base cast material as well as hot-rolled materials has been

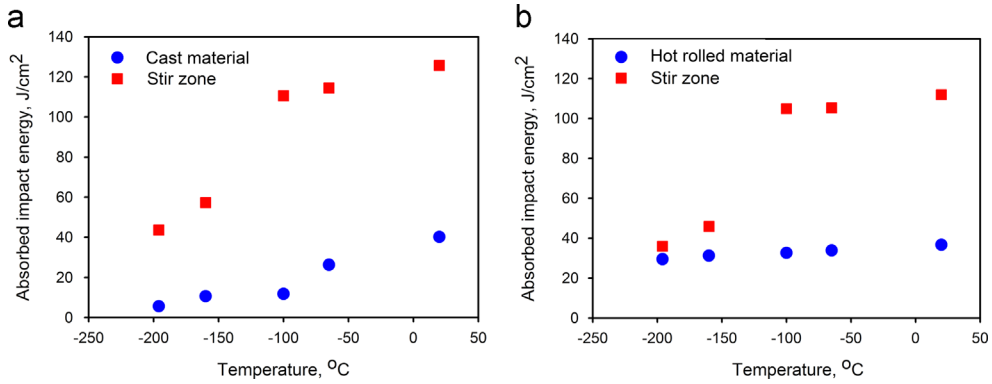


**Fig. 10.** The effect of temperature on the absorbed impact energy in preprocessed and friction-stir welded materials in cast (a) and hot rolled (b) conditions. See Section 3.3.3 for details.

considered in detail in a previous work [2]. Briefly, both materials exhibited dimple rupture at ambient temperature (Fig. 9a and c), thus indicating ductile transgranular fracture. With decreasing temperature, however, a transition towards brittle intergranular fracture was observed; this effect was most pronounced in the cast material (Fig. 9b and d). In this material condition, the fracture was suggested to be related closely with coarse $Al_6Mn$ particles arranged along the original grain boundaries (Fig. 1b).

In the tensioned stir zone material, the fracture surface was found to be broadly similar in both preprocessed material conditions (i.e., cast and hot-rolled ones). For simplicity, therefore, only the fractography of the friction-stir welded cast material is shown in Fig. 9e and f. Over the entire temperature range, the rupture surface seemed to be of dimple type, thus indicating a prevalence of the ductile transgranular fracture mode. Moreover, the dimple size was found to be considerably smaller than that in the base materials, thus reflecting a relatively large resistance to crack nucleation and propagation. The latter effect is thought to be related to the fine-grained nature of the stir zone material (Fig. 3), which may hamper crack propagation.

### 3.3.3. *Impact fracture toughness*

The influence of cryogenic temperatures on the dynamical behavior of the obtained welds is presented in Fig. 10. It is evident from the figure that the stir zone exhibited much higher impact fracture toughness than did the base material at all studied temperatures. Remarkably, the toughness in both friction-stir welded conditions – cast and rolled ones – were broadly similar to each other (Fig. 10). This observation agrees with the microhardness and tensile tests discussed above.

In the cast and stir zone conditions, the impact fracture toughness considerably reduced for temperatures below $\sim -100$ °C (Fig. 10), thus indicating the ductile-to-brittle transition. On the other hand, the hot-rolled material exhibited no significant changes over the entire temperature range (Fig. 10b).

To obtain a deeper insight into the fracture mechanism, rupture surfaces were examined (Fig. 11). Again, the fractography of the stir zone material was found to be broadly similar in both studied material conditions; for simplicity, only the fractured surfaces of the stir zone in the hot-rolled material are shown in Fig. 11e and f.

In the cast material, the observed embrittlement for temperatures below $-65$ °C (Fig. 10a) was accompanied by a fundamental change of the fracture morphology. In the specimens tested at higher temperatures, the fracture surface had a dimpled appearance (Fig. 11a), whereas that for the lower temperatures was distinctly intergranular in nature (Fig. 11b). Similar to the tensions tests discussed in the previous section, the intergranular character of the crack propagation at low temperatures is thought to be related to the grain-boundary network of coarse $Al_6Mn$ particles (Fig. 1b).

In the hot-rolled condition, the transgranular fracture mode was apparently predominant in all of the studied temperatures (Fig. 11c and d). Moreover, the dimples appear to be essentially refined. Although some evidence of intergranular fracture is also observed at cryogenic temperatures (Fig. 11d), this effect was less pronounced than that in the cast condition. The relative insensitivity of the fracture toughness of the hot-rolled material to the test temperature (Fig. 10b) is believed to be associated with the relatively high initial dislocation density (Fig. 1c) that enables the efficient relaxation of the stress at the crack tip. This stress relaxation may also be contributed by the developed subboundary network (Fig. 1c), which may promote crack branching. The detachment of the original grain boundaries from the coarse $Al_6Mn$ particles in the hot-rolled material reported in Ref. [2] may also enhance the crack propagation resistance.

In the stir zone material, the fracture surface also appeared to have a dimpled appearance, thus indicating a predominance of the transgranular fracture mode over the entire temperature range (Fig. 11e and f). The smallest dimple size ($\sim 1$ μm) among all of the studied material conditions appears to be directly related with the highest fracture toughness observed in the stir zone (Fig. 10). In turn, the fine dimple size was obviously associated with the fine-grained nature of the stir zone material (Fig. 3). Therefore, the highest crack propagation resistance in the stir zone is thought to be attributable to drastic grain refinement during the FSW process.

The abrupt decrease of the fracture toughness of the cast material as well as the stir zone materials below $\sim -100$ °C is not completely clear. One of the possible explanations may be the relatively low initial dislocation density for both conditions, which prevented rapid stress relaxation. If so, the material embrittlement observed below $-100$ °C may be associated with the suppression of cross-slip dislocation multiplication, as proposed in the previous section.

## 4. Discussion

FSW highly improves the mechanical properties of the 1575C Al in the as-cast and hot-rolled conditions at both cryogenic and ambient temperatures. It is important to emphasize that FSW leads to a concurrent increase in strength and ductility/fracture toughness, which are the key mechanical properties of structural materials for cryogenic applications [18,19]. These properties typically have opposing characteristics. Materials subjected to intense plastic straining in conventional deformation processing techniques, such as rolling, extrusion and equal channel angular extrusion, may demonstrate superior strength [20]. However, thermo-mechanical

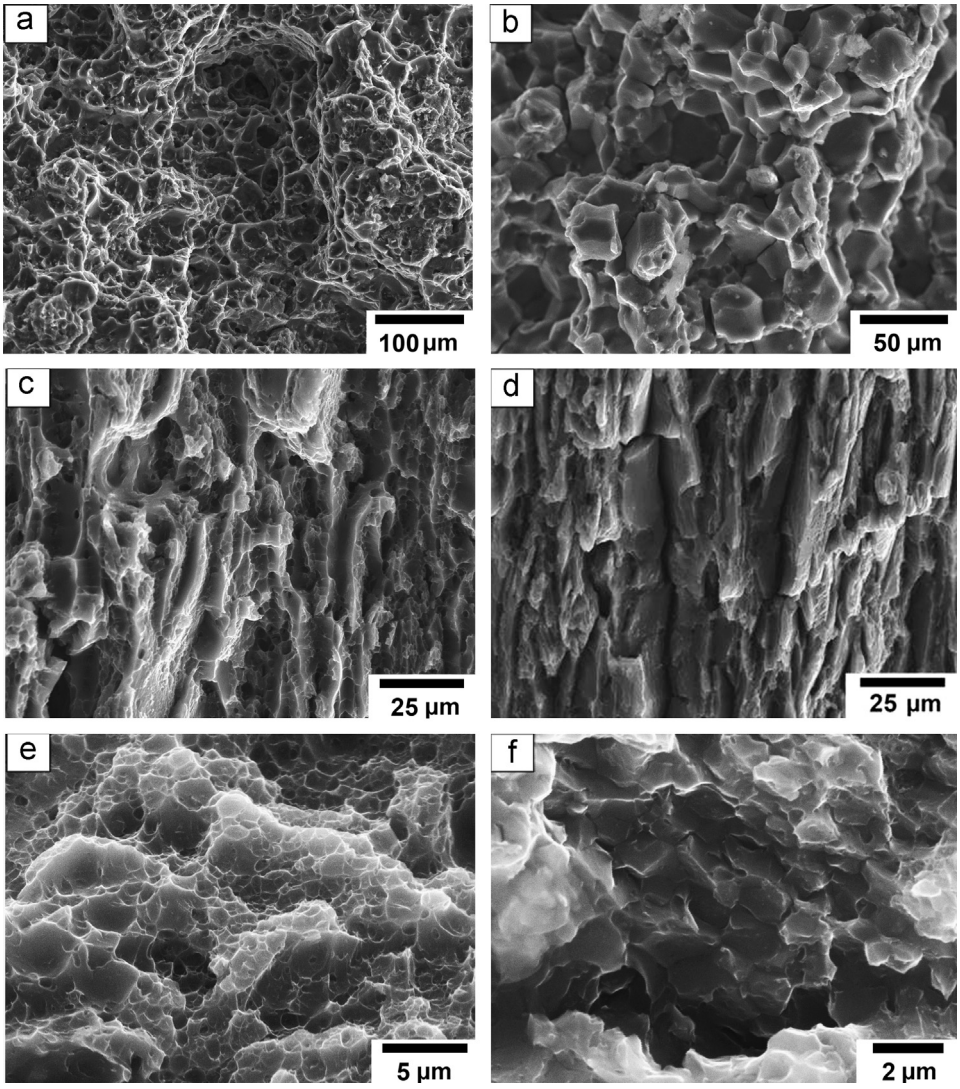


**Fig. 11.** SEM micrographs illustrating the effect of temperature on the fracture surface of the impact specimens: cast material tested at 20 °C (a) and −196 °C (b), hot-rolled material tested at 20 °C (c) and −196 °C (d), friction-stir welded hot-rolled material tested at 20 °C (e) and −196 °C (f). See Section 3.3.3 for details.

processing leads to a concurrent reduction in the ductility and fracture toughness [20]. Aluminum alloys subjected to plastic straining may be strong or ductile, but they are rarely both [20]. Therefore, the positive effect of FSW on the mechanical properties of 1575C Al is unique. This positive effect is attributed to the formation of micron scale grains containing a moderate density of lattice dislocations in the stir zone and coherent dispersoids, which provide sufficient probability of dislocation trapping within the grain interior under tension. As a result, the material in the stir zone exhibits a relatively high strain hardening rate (Fig. 7) that is important to sustain plastic stability. Thus, the formation of fully recrystallized structure in the SZ concurrently enhances the strength, ductility and fracture toughness providing high joint efficiency.

A significant enhancement of the mechanical properties of 1575C Al due to the extensive grain refinement was observed at the cryogenic temperatures at which the full strength joint welds are achieved by FSW. The strength is attributed to suppression of the brittle intergranular fracture along the grain boundaries. Plastic deformation occurs uniformly, and rupture occurs through ductile transgranular fracture that provides concurrent enhancement of the strength and the ductility/fracture toughness. It is obvious that the formation of a fully recrystallized structure in the SZ highly raises the brittle fracture stress, but does not eliminate the ductile-to-brittle transition (DBT) [21]. However, FSW is highly effective in the enhancement of fracture toughness at cryogenic temperatures by the extensive refinement of the "effective grain size," that is, to decrease the mean free path of a crack before a grain boundary or other crystallographic discontinuity forces it to deviate or stop [22]. Therefore, as in steel [21], in the non-age hardenable aluminum alloy, the combination of the ultra-fine grained structure with the dispersion of nanometer-sized particles can lead to the superior combination of high strength with enhanced toughness and ductility at cryogenic temperatures. FSW is highly attractive for producing a lightweight cryogenic structure from high-strength Al–Mg alloys containing a dispersion of coherent precipitates of the $Al_3(Sc,Zr)$ phase.

## 5. Conclusions

In this study, the tensile strength and impact fracture toughness of Al–Mg–Sc–Zr friction-stir joints was examined in the temperature range from 20 °C to −196 °C. To develop a broader view of the weld properties of this alloy, the material was studied

in two commercially available conditions, i.e., cast and hot-rolled conditions. The main conclusions from this work are as follows.

(1) The microstructures evolved in the stir zone were found to be broadly similar for both material conditions. In all cases, the microstructure was dominated by completely recrystallized fine grains ($\sim$1 μm) with low dislocation density ($\sim 2.5 \times 10^{13}$ $m^{-2}$) and a large fraction of high-angle boundaries ($\sim$95%). The constituent nanoscale $Al_3Sc$ dispersoids were preserved in the stir zone, whereas the continuous grain-boundary network of coarse $Al_6Mn$ particles inherent to the cast material was broken down.
(2) In the cast material, FSW imparted a local strengthening effect in the stir zone. As a result, the produced welds were fractured in the base material region during transverse tensile tests and the joint efficiency for yield strength was close to 100% at all of the studied temperatures.
(3) In the hot-rolled condition, the joint efficiency during transverse tensile tests was found to be dependent on the test temperature. In the temperature range from 20 °C to −100 °C, the welds were fractured in the stir zone, and the joint efficiency was ~95%. The subtle material softening in the stir zone was attributed to the elimination of the initial work-hardened microstructure due to recrystallization during the FSW process. At temperatures below −100 °C, however, the joints failed in the base material region, and the joint efficiency achieved 100%. The observed strengthening of the stir zone material in this low temperature range was suggested to be related to the suppression of cross slip and the related difficulty of dislocation multiplication.
(4) The material in the stir zone exhibited superior impact fracture toughness in all of the studied material/temperature conditions. This effect was attributed to the drastic grain refinement as well as the breaking of the continuous grain-boundary network of the coarse $Al_6Mn$ particles during the FSW process.

## Acknowledgments

Financial support from the Ministry of Education and Science of the Russian Federation (Project 14.A18.21.0760) is gratefully acknowledged. The authors also thank the staff of the Joint Research Center at Belgorod State University for their technical assistance.

## References

[1] K.L. Kendig, D.B. Miracle, Acta Mater. 50 (2002) 4165–4175.
[2] D. Zhemchuzhnikova, A. Mogucheva, R. Kaibyshev, Mater. Sci. Eng. A 565 (2013) 132–141.
[3] Cabello Munoz, G. Ruckert, B. Huneau, X. Sauvage, S. Marya, J. Mater. Process. Technol. 197 (2008) 337–343.
[4] J. Zhao, F. Jiang, H. Jian, K. Wen, L. Jiang, X. Chen, Mater. Des. 31 (2010) 306–311.
[5] X. Sauvage, A. Dede, A. Cabello Munoz, B. Huneau, Mater. Sci. Eng. A 491 (2008) 346–371.
[6] P. Yongyi, Y. Zhimin, L. Xuefeng, P. Qinglin, H. Zhenbo, Rare Met. Mater. Eng. 40 (2011) 201–204.
[7] N. Kumar, R.S. Mishra, Mater. Charact. 74 (11) (2012) 1–10.
[8] F.C. Liu, Z.Y. Ma, Scr. Mater. 59 (2008) 882–885.
[9] F.C. Liu, Z.Y. Ma, L.Q. Chen, Scr. Mater. 60 (2009) 968–971.
[10] F.C. Liu, Z.Y. Ma, Scr. Mater. 62 (2010) 125–128.
[11] F.C. Liu, Z.Y. Ma, Mater. Sci. Eng. A 530 (2011) 548–558.
[12] N. Kumar, R.S. Mishra, C.S. Huskamp, K.K. Sankaran, Scr. Mater. 64 (2011) 576–579.
[13] N. Kumar, R.S. Mishra, C.S. Huskamp, K.K. Sankaran, Mater. Sci. Eng. A 528 (2011) 5883–5887.
[14] F.C. Liu, P. Xue, Z.Y. Ma, Mater. Sci. Eng. A 547 (2012) 55–63.
[15] F.C. Liu, Z.Y. Ma, F.C. Zhang, J. Mater. Sci. Technol. 28 (11) (2012) 1025–1030.
[16] J.G. Morris, Mater. Sci. Eng. 5 (5) (1970) 299–302.
[17] D.J. Lloyd, H. Jin, Mater. Sci. Eng. A 585 (2013) 455–459.
[18] N. Oiwa, T. Iijima, A. Kida, S. Ohga, J. Light Met. Weld. Constr. 49 (2011) 2–6.
[19] I.J. Polmear, Light Alloys. From Traditional Alloys to Nanocrystals, fourth ed., Butterworth-Heinemann/Elsevier, UK, 2006.
[20] R.Z. Valiev, T.G. Langdon, Prog. Mater. Sci. 51 (2006) 881–981.
[21] Y. Kimura, T. Inoue, F. Yin, K. Tsuzaki, Science 320-5879 (2008) 1057–1060.
[22] J.W. Morris , Science 320 (2008) 1022–1023.